Nature of the metallic and in-gap states in Ni-doped SrTiO_3

Fatima Alarab, Karol Hricovini, Berengar Leikert, Christine Richter, Thorsten Schmitt, Michael Sing, Ralph Claessen, Ján Minár, Vladimir N Strocov

APL Materials

RESEARCH ARTICLE | JANUARY 22 2024

Nature of the metallic and in-gap states in Ni-doped $SrTiO_3$

Fatima Alarab ; Karol Hricovini ; Berengar Leikert ; Christine Richter ; Thorsten Schmitt; Michael Sing ; Ralph Claessen ; Ján Minár ; Vladimir N. Strocov

APL Mater. 12, 011118 (2024)
https://doi.org/10.1063/5.0183140

Nature of the metallic and in-gap states in Ni-doped $SrTiO_3$

Cite as: APL Mater. 12, 011118 (2024); doi: 10.1063/5.0183140
Submitted: 21 October 2023 • Accepted: 26 December 2023 •
Published Online: 22 January 2024

Fatima Alarab,[1,a] Karol Hricovini,[2] Berengar Leikert,[3] Christine Richter,[2] Thorsten Schmitt,[1] Michael Sing,[3] Ralph Claessen,[3] Ján Minár,[4,a] and Vladimir N. Strocov[1,a]

AFFILIATIONS

[1] Swiss Light Source, Paul Scherrer Institute, 5232 Villigen-PSI, Switzerland
[2] Université Paris-Saclay and CY Cergy Paris Université, CEA, LIDYL, 91191 Gif-sur-Yvette, France
[3] Physikalisches Institut and Würzburg-Dresden Cluster of Excellence ct.qmat, Julius–Maximilians-Universität, 97074 Würzburg, Germany
[4] New Technologies Research Centre, University of West Bohemia, 301 00, Plzeň, Czech Republic

[a] **Authors to whom correspondence should be addressed:** fatima.alarab@psi.ch; jminar@ntc.zcu.cz; and vladimir.strocov@psi.ch

ABSTRACT

Epitaxial thin films of $SrTiO_3$(100) doped with 6% and 12% Ni are studied with resonant angle-resolved photoelectron spectroscopy at the Ti and Ni $L_{2,3}$-edges. We find that the Ni doping shifts the valence band of n-doped pristine $SrTiO_3$ toward the Fermi level (in the direction of p-doping) and reducing the bandgap. In the Ti t_{2g}-derived mobile electron system (MES), the Ni doping depopulates the out-of-plane $d_{xz/yz}$-derived bands, transforming the MES to two-dimensional and progressively reduces the electron density embedded in the in-plane d_{xy}-derived bands as reflected in their Fermi momentum. Furthermore, the Ti and Ni $L_{2,3}$-edge resonant photoemission is used to identify the Ni 3*d* impurity state in the vicinity of the valence-band maximum and decipher the full spectrum of the in-gap states originating from the Ni atoms, Ti atoms, and from their hybridized orbitals. Our experimental information about the dependence of the valence bands, MES, and in-gap states in Ni-doped $SrTiO_3$ may help the development of this material toward its device applications associated with the reduced optical bandgap.

I. INTRODUCTION

Transition metal oxides exhibit a diversity of exotic physical properties, including superconductivity, ferromagnetism, ferroelectricity, etc.,[1] which can potentially be harnessed for emerging applications in electronic and quantum devices. The prototype perovskite complex oxide $SrTiO_3$ (STO) has, in recent decades, been the subject of intensive research both experimentally and theoretically. Quite a few fundamental quantum phenomena, such as 2-dimensional electron conductivity,[2] magnetism, and superconductivity,[3–7] meet in this material, promising novel device functionalities. A novel promise of STO is its use for photocatalysis.[8]

The primary limitation of STO for photocatalytic applications is its large bandgap (>3 eV), which restricts light absorption to the ultraviolet range. Doping of STO with Ni (STO:Ni), where Ni substitutes Ti atoms, induces a slight reduction in the bandgap, thus extending the optical absorption edge toward visible light.[9,10] Furthermore, the Ni doping introduces a spectrum of in-gap states, which radically change the photoabsorption and photoluminescence properties of STO to polychromic.[9] Similar physical phenomena are known, for example, for STO doped with oxygen vacancies (V_Os), whereby its photoluminescence spectrum can be varied from red[11] to blue.[12] Further prospects for STO:Ni can be connected with the Rashba splitting at the surfaces and interfaces of STO-based materials.[13–18] This phenomenon, particularly pronounced at the $LaAlO_3$/STO interfaces, may find a practical application for the spin-charge interconversion through the Edelstein and inverse Edelstein effects.[19–21] Ni-doping can affect this interconversion through the breaking of the Kramers's degeneracy via the magnetic field and through modulation of spin–orbit coupling field interplaying with the Rashba splitting.

The nature of the electronic states in STO:Ni and their evolution upon increasing Ni doping are largely unexplored. For instance, our density-functional theory (DFT) calculations of the partial density of states (PDOS) reveal an energy overlap between the Ti-derived and Ni-derived states in the STO bandgap, which has been confirmed by resonant photoemission (ResPE) data at the Ti and Ni $L_{2,3}$-edges.[10] At the same time, the formation of the MES at the surface of STO:Ni and the effects of Ni doping on its fundamental electronic properties, such as band order and band filling, have not yet been explored, to the best of our knowledge. There are many other aspects of the Ni-doping influence on the fundamental electronic structure of STO, including the in-gap states, which still remain open.

Here, we aim to understand the influence of Ni doping on the electronic structure of STO:Ni thin films ranging from the VB to the continuum of the in-gap states and the MES in the vicinity of the Fermi level (E_F). By employing Ti and Ni $L_{2,3}$-edge resonant ARPES, we attempt to explore the elemental character and orbital hybridization through the whole electronic structure. Our investigation includes STO(100) single crystal as the pristine reference material.

II. EXPERIMENTAL DETAILS

We employed the pulsed laser deposition (PLD) technique to achieve epitaxial growth of STO:Ni_x films with varying Ni concentrations (x = 0.06 and 0.12). A principal challenge in fabricating STO:Ni films lies in the successful substitution of Ni cations into the STO lattice sites. The calculated formation energy for STO:Ni reveals a preference for Ni atoms to substitute Ti cations (7.8 eV for Ni at Ti sites) over Sr cations (9 eV for Ni at Sr sites).[22] However, this value remains quite high due to the very limited solubility of Ni within STO, favoring the formation of metal clusters within the host lattice.[23] To mitigate Ni clustering and promote oxidation toward the Ni^{x+} state ($2 < x < 4$), we employed a pressed and sintered target fabricated from mixed $[SrTiO3]_{1-x}/[NiO]_x$ powder with x = 6 and 12 at. %. The thin films were deposited onto TiO_2-terminated (100) surfaces of niobium-doped (5 at. %) STO substrates. Our optimization process identified substrate temperatures of 700 °C, laser energy of 1.8 J/cm^2, and an oxygen background gas pressure of $1 \cdot 10^{-1}$ mbar. Deposition was ceased after growing 11 units of cells on each substrate. The structural characterization data of the films have been detailed,[10] confirming the successful substitution of Ni ions into the Ti sites of STO. The insignificant concentration, if not absence, of the Ni clusters in our samples is confirmed by the Ni $L_{2,3}$-edge x-ray absorption (XAS) and ResPE spectra (see below) that do not show any discernible contribution from metallic Ni. This is also confirmed by clear LEED and RHEED patterns as well as sharp **k**-resolved ARPES spectra of our samples, which also evidence an insignificant concentration of NiO_x phases.

Considering the ex-situ transfer of all samples to the experimental endstation, a surface cleaning protocol was required to mitigate surface contamination. This involved ozone etching of the samples, followed by thermal annealing in a vacuum of $2 \cdot 10^{-9}$ mbar at 300 °C for 30 min. The same treatment was applied to both the STO:Ni films and the bare STO substrate, serving as our reference sample.

XAS, ResPE, and ARPES measurements were conducted at the soft x-ray ARPES endstation of the ADRESS beamline at the swiss light source.[24,25] Circularly polarized incident light was employed. The analyzer slit was oriented in the plane formed by the incident light, and the surface was normal (for details of the experimental geometry, see Ref. 24). The spot size on the sample was around ~30 × 75 μm^2. An ultrahigh vacuum of $\sim 1 \cdot 10^{-10}$ mbar and a sample temperature of 12 K were maintained during the experiment. As x-ray irradiation can generate V_Os in STO-based samples, leading to their effective n-doping, the measurements were performed at saturation of the spectra after ~1 h of irradiation. For all experimental ARPES images presented, the coherent spectral fraction, reduced by the Debye–Waller factor,[26] was enhanced by subtracting the angle-integrated spectrum. The ResPE spectra were acquired at the Ti and Ni $L_{2,3}$-edges ($2p \rightarrow 3d$ resonances) to selectively enhance the signal originating from the Ti 3d and Ni 3d derived electron states, respectively. The normal-emission angle (Γ-point in the k_x direction along the analyzer slit) was set from the d_{xy} dispersions measured at a Ti-resonance excitation energy of 457.4 eV.

III. RESULTS AND DISCUSSION

A. Ti $L_{2,3}$-edge resonant photoemission

Bulk STO is a band insulator with a large bandgap of 3.2 eV. Under x-ray irradiation, however, it develops surface conductivity where the Ti 3d t_{2g} derived conduction-band (CB) states become populated to form the MES (effective n-doping). In the presence of the surface breaking the degeneracy of the bulk t_{2g} states, they split into the ones derived from the in-plane d_{xy} orbital and the ones derived from the out-of-plane $d_{xz/yz}$ orbitals (for brevity, we will neglect the cubic to tetragonal phase transition in STO at 105 K because the corresponding atomic displacements are relatively small[27] and keep using the cubic notation for symmetry). It is generally accepted that the formation of this MES is attributed to the formation of V_Os. In this case, one of the two electrons is released by the Ti atom to join the MES, and another stays localized at the Ti atom to form an in-gap state. The latter is derived from the Ti 3d e_g states shifted down in energy due to strong electron correlations (for a detailed picture, see Refs. 28–30 and the references therein). A qualitative difference between STO:Ni and its pristine counterpart is that it contains Ni derived impurity states in the gap,[10] and the V_Os generated by x-ray irradiation can only modify them and induce additional Ti 3d e_g derived ones.

To capture the nature of the MES and in-gap states in STO and STO:Ni, we have performed ResPE measurements through the Ti and Ni $L_{2,3}$-edge resonances. Figures 1(a) and 1(b) display our results for the former as ARPES intensity maps $I(E_B,h\nu)$ for both STO crystal and STO:$Ni_{0.06}$ films, plotted as a function of binding energy (E_B, in the negative-sign notation) and excitation energy ($h\nu$). In this map, $I(E_B, h\nu)$ was integrated within $k_x = \pm 0.1$ Å^{-1} in order to enhance the signal from the MES states centered at Γ compared to the spectra integrated over the whole angular acceptance of the analyzer.

For pristine STO, Fig. 1(a), the ResPE map reveals the resonating Ti 3d weight distributed over (1) the VB, composed of the O 2p states hybridized with Ti 3d; (2) the in-gap states, with a well-defined Ti 3d impurity state at $E_B \sim -1.15$ eV derived from

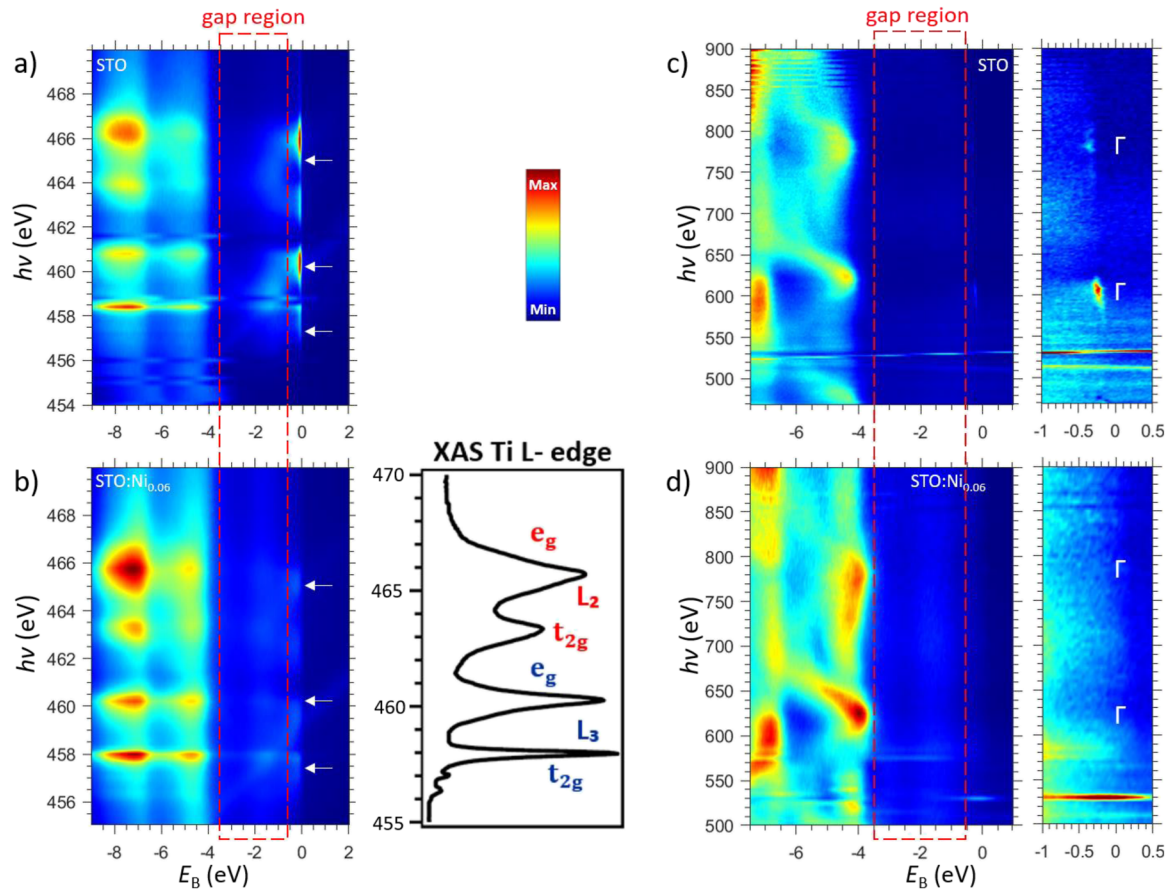

FIG. 1. *hv*-dependent ARPES of STO and STO:Ni. (a) and (b) ResPE intensity maps in the VB of (a) pristine STO and (b) STO:$Ni_{0.06}$ films for *hv* varying through the Ti $L_{2,3}$-edge, with the corresponding XAS spectrum. The white arrows indicate the *hv* values at which the ARPES maps in Fig. 2 are taken. (c) and (d) *hv* scan in an extended range above the Ti resonance, showing the out-of-plane band dispersions of (c) STO and (d) STO:$Ni_{0.06}$ films (the narrow and weak Ni $L_{2,3}$-edge resonance is not well shown). In addition, displayed is their zoom-in around E_F, showing the MES signal blowing up at k_z in the Γ-points.

the Ti 3*d* e_g states brought down in energy because of strong correlations;[28–30] and (3) the MES in the vicinity of E_F, derived from the Ti 3*d* t_{2g} states.[28–30] The resonance of the t_{2g}-derived MES appears at somewhat higher *hv* compared to the t_{2g} peak in XAS, which can be explained by remnant **k**-conservation in the ResPE process.[28]

Turning to STO:$Ni_{0.06}$ in Fig. 1(b), the Ti $L_{2,3}$-edge XAS spectrum is hardly distinguishable from that of pristine STO.[28–30] With its main peaks labeled, the spectrum exhibits the same features in the STO case:[31,32] the spin–orbit splitting of the L_3-and L_2-edges and the crystal-field splitting into t_{2g} and e_g, orbitals. In the ResPE map, however, we observe that the Ti 3*d* in-gap state is shifted from E_B = −1.15 to −1.4 eV. Furthermore, the whole in-gap spectral intensity and the MES signal were significantly reduced in comparison with the STO case. As we will see below, the latter is consistent with the depopulation of the $d_{xz/yz}$ states penetrating deeper into the STO bulk compared to the d_{xy} ones located closer to the surface.

B. Three-dimensional electronic structure

The map in Figs. 1(c) and 1(d) covers an extended *hv* region above the Ti $L_{2,3}$-edge resonance. Again, $I(E_B, hv)$ in this map was integrated within k_x = ±0.1 $Å^{-1}$. The dispersing ARPES peaks reflect the VB dispersions as a function of the out-of-plane momentum k_z. Turning to the MES signal in the STO map, Fig. 1(c), we note that in the shown *hv* region above 500 eV, the photoelectron inelastic mean free path λ_{PE} is relatively large. Therefore, the MES signal here comes predominantly from the out-of-plane $d_{xz/yz}$ states because their larger extension into the bulk compared to the in-plane d_{xy} derived ones provides a larger overlap with the final state extending over λ_{PE}. The signal from the MES appears at *hv* = 605 and 780 eV, where k_z is around the Γ-points.[33] This observation is consistent with the three-dimensional (3D) nature of the $d_{xz/yz}$ states in the MES induced by the V_Os. We also notice that the Ni doping shifts the VB by ~0.5 eV toward the E_F and reduces the bandgap by ~0.4 eV. This shift is consistent with another effect of the Ni doping discussed below: the depopulation of the out-of-plane

$d_{xz/yz}$-derived states and, thus, the vanishing of the off-resonance MES signal.

C. Ni-concentration dependence of the mobile electron system

Ti $L_{2,3}$-edge resonant ARPES images of the VB and CB states for the pristine STO and STO:Ni samples, measured at a few representative excitation energies marked in Figs. 1(a) and 1(b), are displayed in Fig. 2. We will now follow their evolution with the Ni concentration.

All maps for the STO sample in Fig. 2(a) and the STO:$Ni_{0.06}$ and STO:$Ni_{0.12}$ ones in (b) and (c), respectively, show dispersive bulk bands located within an E_B range of −4–9 eV, arising from the O 2*p* states. The d_{xy}-derived and $d_{xz/yz}$-derived bands, constituting the MES in the vicinity of E_F, are located near the Γ-point. To effectively differentiate the light d_{xy} band from the heavy d_{yz} ones (see Ref. 28), we used three *hv* values going through the t_{2g} and e_g states of the L_3 and L_2 edges. The first observation is that the MES to VB intensity ratio for the STO:Ni samples is nearly an order of magnitude smaller compared to the STO one [note the different intensity scales in the MES and VB energy regions in (a)]. As we will see below, the Ni doping depopulates the $d_{xz/yz}$ states, giving a maximal contribution to the MES signal. The concomitant reduction of the MES intensity apparently scales the VB intensity in our

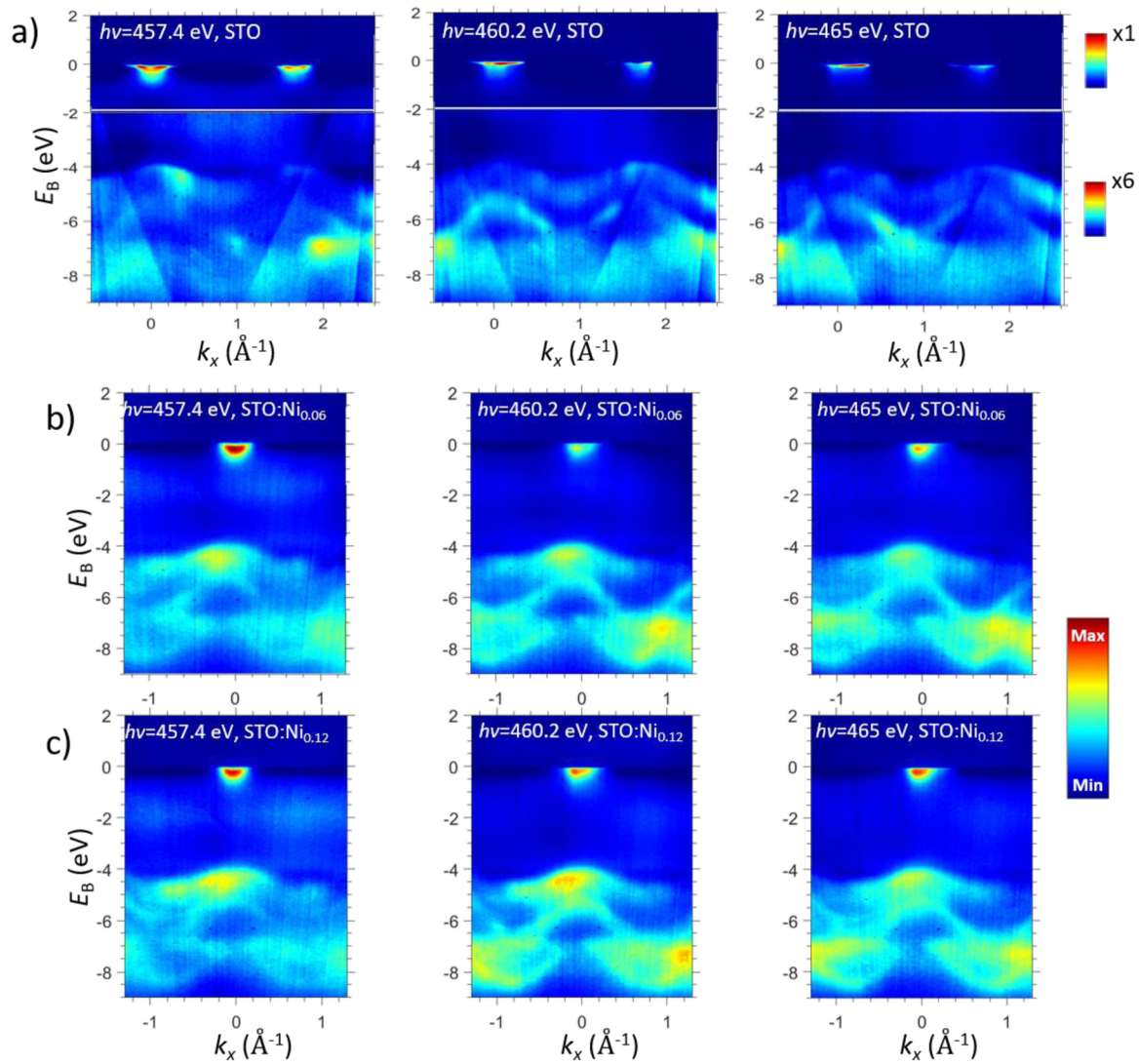

FIG. 2. Resonant ARPES at *hv* selected at the Ti L_3 (t_{2g}), L_3 (e_g), and L_2 (e_g) XAS peaks marked with arrows in Figs. 1(a) and 1(b): (a) STO crystal (note different intensity scales within the VB and CB regions; the inclined lines are electron optics artifacts enhanced by the background subtraction), and (b) STO:$Ni_{0.06}$ and STO:$Ni_{0.12}$ films. The MES to VB intensity ratio reduces under Ni doping because of the depopulation of the $d_{xz/yz}$ states.

ARPES images, where the color scale is normalized to the maximal intensity.

Figures 3(a)–3(c) zoom into the MES regions in Figs. 2(a)–2(c), respectively. One can clearly see the light d_{xy} bands and the heavy d_{yz} ones (the light d_{xz} bands degenerate with the d_{yz} ones in the Γ-point and are hardly visible on top of the d_{yz} intensity). The first observation here is that whereas the d_{xy} band is visible for all samples at all excitation energies, the d_{yz} one fades away with Ni doping and can be marginally seen only at $h\nu$ = 465 eV, where the d_{yz} to d_{xy} intensity ratio is maximal.[28] This depopulation of the d_{xz}/d_{yz} bands, fully developing already at small Ni concentrations, evidences that the MES in Ni-doped STO becomes two-dimensional (2D). Interestingly, the energy position and dispersion of the remnant d_{yz} signal closely resemble the d_{yz} band of pristine STO; this fact may indicate spatial fluctuations of the Ni concentration in our STO:Ni samples where, in the spirit of the phase-separation picture, a small volumetric fraction would stay nearly pristine.

Our second observation in Figs. 3(a)–3(c) is about the electron concentration in the d_{xy} band, expressed by the Luttinger count of the corresponding Fermi surface sheet. We have extracted the corresponding k_F values as a function of Ni doping from the momentum-distribution-curve (MDC) cuts of the spectral intensity $W(k)$ integrated within a 50 meV range around E_F, Fig. 3(d), where the extremes of its gradient dW/dk identify the k_F values.[33–35] We find them systematically decrease from 0.20 Å^{-1} in pristine STO to 0.15 Å^{-1} upon 12% Ni doping. At the same time, interestingly, we find that the bottom of the d_{xy} band stays at nearly the same E_B ~ 250 meV (within an experimental accuracy of ±15 meV), whereby the d_{xy} effective mass (m^*) progressively reduces from ~$0.7m_0$ in pristine STO to ~$0.55m_0$ in STO:Ni$_{0.06}$ and ~$0.35m_0$ in STO:Ni$_{0.12}$, where m_0 is the free-electron mass. Simultaneously, we observe a significant increase in the energy broadening of these states, manifesting a higher electron scattering rate on the total number of Ni atoms as defects in STO. This additional scattering would prohibit an increase in electron mobility potentially associated with a reduction of m^*. In this connection, we should mention the Mn doping of the $LaAlO_3$ (LAO) overlayer at the LAO/STO interfaces,[35] which also reduces the electron density in the MES. In that case, however, its spatial separation from the Mn dopant atoms inhibits the associated defect scattering and allows an electron-mobility boost. We note that the observed shift of the d_{xz}/d_{yz} bands above E_F and the nearly constant energy position of the d_{xy} one, associated with progressive reduction of its m^*, reveal complex physics of Ni doping of STO beyond the conventional rigid-shift model. The different responses of the d_{xz}/d_{yz} and d_{xy} states to the Ni doping may be attributed to their wavefunction being extended over the band-bending region at the surface or localized in the surface layer, respectively.

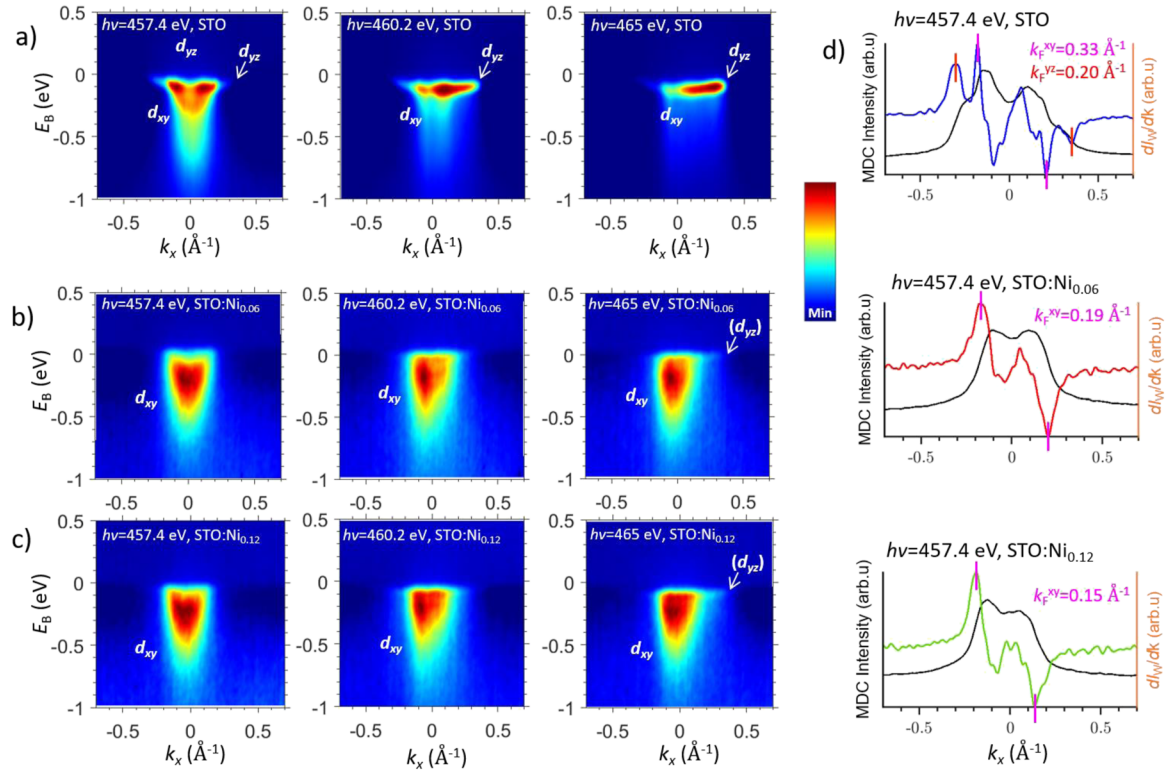

FIG. 3. Effect of Ni doping on the resonant ARPES of the MES: (a) STO crystal, (b) STO:Ni$_{0.06}$, and (c) STO:Ni$_{0.12}$ films (zoom-in of the data in Fig. 2). (d) MDC cuts at $h\nu$ = 457.4 eV (integrated within E_F ± 50 meV) and the corresponding gradient dW/dk (color lines) of the bandwidth-integrated intensity $W(k)$ (black). The maxima/minima of dW/dk, marked by the red and purple vertical lines, identify the k_F values for the d_{xy} and d_{yz} bands, whose numerical values are displayed in the corresponding colors.

Another interesting observation in Figs. 3(a)–3(c) is that the MES spectral intensity is notably asymmetric relative to the Γ-point. Such an asymmetry is, in principle, not prohibited because the angle between the surface normal and the x-ray polarization vector light is different for k_x on the opposite sides of Γ; another contribution to the asymmetry is the photon momentum, which is ~0.24 Å^{-1} at the Ti $L_{2,3}$-edge.[33] This effect should be traced back to the different behavior of the d_{xy} and $d_{xz/yz}$ bands across the resonance, vividly discussed in Refs. 28, combined with their gradual depopulation with an increase in Ni doping.

D. Ni $L_{2,3}$-edge resonant photoemission

In our previous work,[10] the origin of the main VB features of the Ni-doped STO films was investigated both experimentally and theoretically by means of (angle-integrated) ResPE and DFT calculations, respectively. In the present work, we deepen this analysis based on a detailed ResPE map $I(E_B, h\nu)$ presented in Figs. 4(a) and 4(c). Here, the VB spectra of STO:Ni$_{0.06}$ and STO:Ni$_{0.12}$ are recorded across the Ni L_3 absorption edge, with $h\nu$ varying from 850 to 856 eV in increments of 0.5 eV. To accentuate the Ni resonant spectral weight, Figs. 4(b) and 4(d) present a map of the differential intensity $\Delta_{res}(E_B, h\nu) = I(E_B, h\nu) - I(E_B, h\nu_0)$ obtained by subtracting, from each $I(E_B, h\nu)$ spectrum, the pre-resonance one $I(E_B, h\nu_0)$ measured at $h\nu_0$ = 850 eV.

Beginning with the XAS spectrum for the STO:Ni$_{0.06}$ case in Fig. 4(a), we note that the main Ni L_3 absorption edge, situated at 853.3 eV, is followed by a weaker peak around 855 eV. The latter is attributed to multiplet splitting of the $2p^5 3d^9$ state, connected with the strongly correlated nature of Ni-ions in the crystal field.[10] In the corresponding ResPE map across the Ni L_3 edge ($h\nu$ from 852.5 to 853.5 eV), we observe, first of all, an intensity boost of the whole VB, indicating the hybridization of the O 2p states with the Ni 3d ones. Furthermore, we observe a notable resonance of the whole in-gap spectral range down to the VB maximum (VBM). This resonant behavior is accentuated in the Δ_{res} map (b). Here, we can discern two distinct resonant peaks, where the first manifests the main Ni 3d impurity state at E_B of −3.5 eV (~0.5 eV above the VBM)[36] and the second a Ni-derived in-gap state at −1.9 eV. While with an increase in $h\nu$, all these resonant structures stay at constant E_B, which is characteristic of the coherent resonant photoemission process, we note a feature near the VB bottom that appears at $h\nu$ above the VB resonance and follows a constant-kinetic-energy line. This feature is associated with an incoherent process of resonant Auger decay.[3]

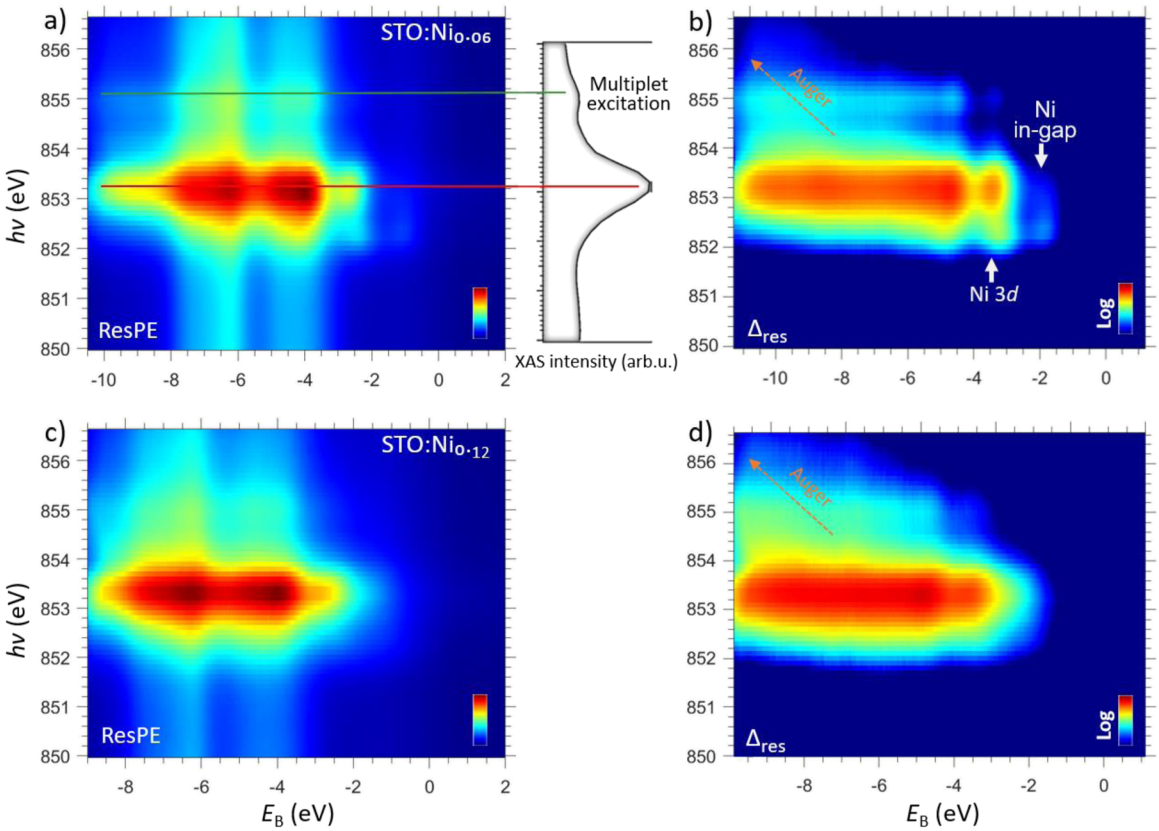

FIG. 4. Ni L_3-edge ResPE intensity data map for (a) STO:Ni$_{0.06}$ and (c) STO:Ni$_{0.12}$ films, with the L_3-edge XAS spectrum for STO:Ni$_{0.06}$ shown in (a). (b) and (d) Differential ResPE maps (logarithmic scale), where the pre-resonant spectrum at $h\nu_0$ = 850 eV is subtracted, for STO:Ni$_{0.06}$ (b) and STO:Ni$_{0.12}$ (d). These maps show the resonant contribution of the Ni states Δ_{res} to the VB spectral weight.

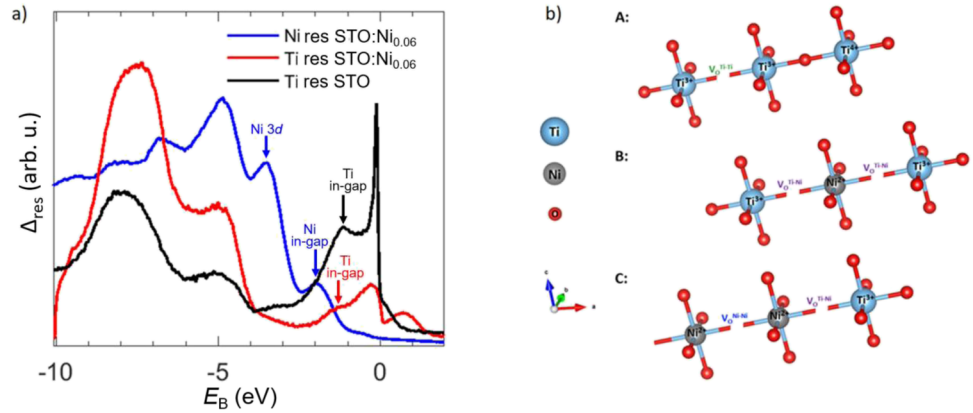

FIG. 5. In-gap states and their orbital configurations. (a) Resonating Fermi states and the in-gap states of (black) pristine STO crystal and (red) STO:$Ni_{0.06}$ films recorded at the Ti $L_3(e_g)$ resonance at $h\nu$ = 460 eV (the peak above E_F comes from the Ti $2p_{3/2}$ core level excited by second-order light from the beamline monochromator) and of (blue) STO:$Ni_{0.06}$ films recorded at the Ni L_3 resonance at $h\nu$ = 853 eV. (b) Atomic configurations of the octahedral in STO:Ni, showing different incorporation of the V_Os relative to the Ti and Ni atoms, leading to different in-gap states.

The experimental ResPE map for the STO:$Ni_{0.12}$ films is presented in Figs. 4(c) and 4(d). As expected, the increase in Ni content produces more pronounced and broader resonant peaks compared to the STO:$Ni_{0.06}$ case. The in-gap state at −1.9 eV is smeared out with the Ni concentration increase. Otherwise, the overall ResPE intensity pattern closely resembles that of STO:$Ni_{0.06}$.

E. Ti- and Ni-derived in-gap states

In the last section, we will focus on the possible origins of in-gap states observed in our STO:Ni samples. Figure 5(a) presents the (angle-integrated) ResPE spectra measured at the Ti(e_g) and Ni L_3 resonances at $h\nu$ = 460 and 853 eV, respectively. In STO, the in-gap states resonate at the Ti edge at E_B = −1.15 eV, similar to the previous reports.[2,28,37] These in-gap states originate from Ti ions located near the V_Os and are often viewed as small polarons.[28] Upon 6% Ni doping, this resonant peak broadens and shifts to E_B = −1.4 eV, suggesting hybridization of these states with the Ni 3*d* ones in STO:Ni. At the Ni resonance, we observe the Ni 3*d* impurity state at E_B ∼ −3.5 eV and the in-gap state at −1.9 eV. This observation consequently suggests the presence of two distinct types of in-gap states in STO:Ni samples. The first type, resonating at the Ti L_3 edge, corresponds to localized charge carriers from the Ti ions near the V_Os, which may hybridize with the Ni dopants. The second type of in-gap states, positioned at −1.9 eV, resonate only at the Ni $L_{2,3}$-edge. Based on the similarity of its energy with the Ti derived in-gap electrons, we attribute them to the V_Os formed within Ni octahedra.

Figure 5(b) illustrates different variants of atomic configurations of the octahedra in STO:Ni, which can incorporate V_Os and, subsequently, generate the diverse in-gap states discussed above. Scheme A reflects the scenario of V_Os linked to Ti^{3+} species, akin to those in pristine STO. Alternatively, scheme B shows their association with both Ti^{3+} and Ni^{2+} ions. Another configuration, outlined in scheme C, shows V_Os surrounded solely by Ni^{2+} ions, ultimately leading to entirely different in-gap states at E_B = −1.9 eV. The electronic configurations and their connection with the electron paramagnetic resonance and photochromic optical absorption for this configuration were discussed in detail by Koidl *et al.*[9]

IV. CONCLUSION

We have explored the delocalized MES and localized in-gap states in STO:$Ni_{0.06}$ and STO:$Ni_{0.12}$ films in comparison with n-doped pristine STO using resonant soft-x-ray ARPES at the Ti and Ni $L_{2,3}$-edges. Our main findings include (1) the 3D band structure of STO:Ni and STO, where the Ni doping shifts the VB by ∼0.5 eV toward E_F (in the direction of p-doping) and reduces the bandgap by ∼0.4 eV; and (2) the doping shifts the out-of-plane $d_{xz/yz}$ states above E_F, depopulating them. A faint remnant weight of these states gives an inkling of Ni doping inhomogeneity. The doping also reduces electron density in the in-plane d_{xy} states, as evidenced by the gradual reduction of the corresponding k_F. The prevalence of the d_{xy} states renders the MES at most 2D. The observed shift of the d_{xz}/d_{yz} bands above E_F at a nearly constant energy position of the d_{xy} one sets the physics of Ni doping of STO beyond the rigid-shift picture typical of conventional semiconductors. (3) The Ni 3*d* impurity state has been identified at ∼0.5 eV above the VBM. Furthermore, the full spectrum of the V_O-induced in-gap states has been identified, including the localized electrons trapped in the 3*d* orbitals of Ni atoms and of Ti ones. The latter shifts by ∼0.25 eV upon the Ni doping as the result of their hybridization with the neighboring Ni atoms. We conjecture that the above modifications of the MES and in-gap electronic spectrum are largely affected by the deformation of the Ti octahedra under the lattice strain induced by Ni doping. The knowledge of the electronic spectrum of the MES and in-gap states in STO:Ni as a function of Ni concentration, achieved in this work, may help tailor the properties of the STO:Ni-based materials to potential device applications.

ACKNOWLEDGMENTS

F.A. acknowledges the financial support from the Swiss National Science Foundation within Grant No. 200020B_188709. This publication was supported by the project QM4ST with Reg. No. CZ.02.01.01/00/22_008/0004572, co-funded by the ERDF as part of the MŠMT. The work in Würzburg was supported by the Deutsche Forschungsgemeinschaft (DFG, German Research Foundation) under Germany's Excellence Strategy through the Würzburg–Dresden Cluster of Excellence on Complexity and Topology in Quantum Matter ct.qmat (EXC 2147, Project No. 390858490) as well as through the Collaborative Research Center SFB 1170 ToCoTronics (Project No. 258499086).

AUTHOR DECLARATIONS

Conflict of Interest

The authors have no conflicts to disclose.

Author Contributions

Fatima Alarab: Data curation (equal); Formal analysis (equal); Methodology (equal); Software (equal); Writing – original draft (equal). **Karol Hricovini**: Conceptualization (equal); Funding acquisition (equal); Investigation (equal); Project administration (equal); Supervision (supporting); Validation (equal). **Berengar Leikert**: Data curation (equal); Investigation (equal); Writing – review & editing (equal). **Christine Richter**: Investigation (equal); Resources (equal); Supervision (equal). **Thorsten Schmitt**: Methodology (equal); Resources (equal); Supervision (equal). **Michael Sing**: Methodology (equal); Resources (equal); Validation (equal); Writing – review & editing (equal). **Ralph Claessen**: Conceptualization (equal); Methodology (equal); Project administration (equal); Resources (equal); Supervision (equal); Writing – review & editing (equal). **Ján Minár**: Conceptualization (lead); Data curation (equal); Formal analysis (supporting); Investigation (equal); Methodology (equal); Project administration (equal); Software (supporting); Supervision (supporting); Validation (equal); Writing – review & editing (equal). **Vladimir N. Strocov**: Data curation (equal); Funding acquisition (equal); Investigation (equal); Methodology (equal); Project administration (equal); Resources (equal); Software (equal); Supervision (equal); Validation (equal); Writing – review & editing (equal).

DATA AVAILABILITY

The data that support the findings of this study are available from the corresponding authors upon reasonable request.

REFERENCES

[1] K. Ueno, S. Nakamura, H. Shimotani, A. Ohtomo, N. Kimura, T. Nojima, H. Aoki, Y. Iwasa, and M. Kawasaki, "Electric-field-induced superconductivity in an insulator," Nat. Mater. **7**, 855–858 (2008).

[2] A. F. Santander-Syro, O. Copie, T. Kondo, F. Fortuna, S. Pailhès, R. Weht, X. G. Qiu, F. Bertran, A. Nicolaou, A. Taleb-Ibrahimi, P. Le Fèvre, G. Herranz, M. Bibes, N. Reyren, Y. Apertet, P. Lecoeur, A. Barthélémy, and M. J. Rozenberg, "Two-dimensional electron gas with universal subbands at the surface of $SrTiO_3$," Nature **469**, 189–193 (2011).

[3] M. N. Gastiasoro, J. Ruhman, and R. M. Fernandes, "Superconductivity in dilute $SrTiO_3$: A review," Ann. Phys. **417**, 168107 (2020).

[4] M. Sing, H. O. Jeschke, F. Lechermann, R. Valentí, and R. Claessen, "Influence of oxygen vacancies on two-dimensional electron systems at $SrTiO_3$-based interfaces and surfaces," Eur. Phys. J.: Spec. Top. **226**, 2457–2475 (2017).

[5] K. Ahadi, L. Galletti, Y. Li, S. Salmani-Rezaie, W. Wu, and S. Stemmer, "Enhancing superconductivity in $SrTiO_3$ films with strain," Sci. Adv. **5**, eaaw0120 (2019).

[6] S. Salmani-Rezaie, L. Galletti, T. Schumann, R. Russell, H. Jeong, Y. Li, J. W. Harter, and S. Stemmer, "Superconductivity in magnetically doped $SrTiO_3$," Appl. Phys. Lett. **118**, 202602 (2021).

[7] G. Scheerer, M. Boselli, D. Pulmannova, C. W. Rischau, A. Waelchli, S. Gariglio, E. Giannini, D. van der Marel, and J.-M. Triscone, "Ferroelectricity, superconductivity, and $SrTiO_3$—Passions of K. A. Müller," Condens. Matter **5**, 60 (2020).

[8] A. Bera, K. Wu, A. Sheikh, E. Alarousu, O. F. Mohammed, and T. Wu, "Perovskite oxide $SrTiO_3$ as an efficient electron transporter for hybrid perovskite solar cells," J. Phys. Chem. C **118**, 28494–28501 (2014).

[9] P. Koidl, K. W. Blazey, W. Berlinger, and K. A. Müller, "Photochromism in Ni-doped $SrTiO_3$," Phys. Rev. B **14**, 2703 (1976).

[10] F. Alarab, K. Hricovini, B. Leikert, L. Nicolaï, M. Fanciulli, O. Heckmann, C. Richter, L. Prušakova, Z. Jansa, P. Šutta, J. Rault, P. Lefevre, M. Sing, M. Muntwiler, R. Claessen, and J. Minár, "Photoemission study of pristine and Ni-doped $SrTiO_3$ thin films," Phys. Rev. B **104**, 165129 (2021).

[11] M. L. Crespillo, J. T. Graham, F. Agullo-Lopez, Y. Zhang, and W. J. Weber, "Isolated oxygen vacancies in strontium titanate shine red: Optical identification of Ti^{3+} polarons," Appl. Mater. Today **12**, 131–137 (2018).

[12] D. Kan, T. Terashima, R. Kanda, A. Masuno, K. Tanaka, S. Chu, H. Kan, A. Ishizumi, Y. Kanemitsu, Y. Shimakawa, and M. Takano, "Blue-light emission at room temperature from Ar^+-irradiated $SrTiO_3$," Nature Mater. **4**, 816–819 (2005).

[13] C. Yin, P. Seiler, L. M. K. Tang, I. Leermakers, N. Lebedev, U. Zeitler, and J. Aarts, "Tuning Rashba spin-orbit coupling at $LaAlO_3/SrTiO_3$ interfaces by band filling," Phys. Rev. B **101**, 245114 (2020).

[14] N. Lebedev, M. Stehno, A. Rana, P. Reith, N. Gauquelin, J. Verbeeck, H. Hilgenkamp, A. Brinkman, and J. Aarts, "Gate-tuned anomalous Hall effect driven by Rashba splitting in intermixed $LaAlO_3/GdTiO_3/SrTiO_3$," Sci. Rep. **11**, 10726 (2021).

[15] S. Noh, D. Choe, H. Jin, and J.-W. Yoo, "Enhancement of the Rashba effect in a conducting $SrTiO_3$ surface by MoO_3 capping," ACS Appl. Mater. Interfaces **14**, 50280–50287 (2022).

[16] D. Q. To, T. H. Dang, L. Vila, J. P. Attané, M. Bibes, and H. Jaffrès, "Spin to charge conversion at Rashba-split $SrTiO_3$ interfaces from resonant tunneling," Phys. Rev. Res. **3**, 043170 (2021).

[17] T. Kim, S.-I. Kim, S.-H. Baek, J. Hong, and H. C. Koo, "Conductance change induced by the Rashba effect in the $LaAlO_3/SrTiO_3$ interface," J. Nanosci. Nanotechnol. **15**, 8632–8636 (2015).

[18] M. H. Fischer, S. Raghu, and E.-A. Kim, "Spin–orbit coupling in $LaAlO_3/SrTiO_3$interfaces: Magnetism and orbital ordering," New J. Phys. **15**, 023022 (2013).

[19] M. Trama, V. Cataudella, C. A. Perroni, F. Romeo, and R. Citro, "Tunable spin and orbital Edelstein effect at (111) $LaAlO_3/SrTiO_3$ interface," Nanomaterials **12**, 2494 (2022).

[20] F. Telesio, R. Moroni, I. Pallecchi, D. Marré, G. Vinai, G. Panaccione, P. Torelli, S. Rusponi, C. Piamonteze, E. di Gennaro, A. Khare, F. Miletto Granozio, and A. Filippetti, "Study of equilibrium carrier transfer in $LaAlO_3/SrTiO_3$ from an epitaxial $La_{1-x}Sr_xMnO_3$ ferromagnetic layer," J. Phys. Commun. **2**, 025010 (2018).

[21] A. Johansson, B. Göbel, J. Henk, M. Bibes, and I. Mertig, "Spin and orbital Edelstein effects in a two-dimensional electron gas: Theory and application to $SrTiO_3$ interfaces," Phys. Rev. Res. **3**, 013275 (2021).

[22] X.-L. Dong, K.-H. Zhang, and M.-X. Xu, "First-principles study of electronic structure and magnetic properties of $SrTi_{1-x}MxO_3$ (M = Cr, Mn, Fe, Co, or Ni)," Front. Phys. **13**, 137106 (2018).

[23] M. Hennes, V. Schuler, X. Weng, J. Buchwald, D. Demaille, Y. Zheng, and F. Vidal, "Growth of vertically aligned nanowires in metal–oxide nanocomposites:

Kinetic Monte-Carlo modeling *versus* experiments," Nanoscale **10**, 7666–7675 (2018).
[24]V. N. Strocov, X. Wang, M. Shi, M. Kobayashi, J. Krempasky, C. Hess, T. Schmitt, and L. Patthey, "Soft-X-ray ARPES facility at the ADRESS beamline of the SLS: Concepts, technical realisation and scientific applications," J. Synchrotron Radiat. **21**, 32–44 (2013).
[25]V. N. Strocov, T. Schmitt, U. Flechsig, T. Schmidt, A. Imhof, Q. Chen, J. Raabe, R. Betemps, D. Zimoch, J. Krempasky, X. Wang, M. Grioni, A. Piazzalunga, and L. Patthey, "High-resolution soft X-ray beamline ADRESS at the Swiss light source for resonant inelastic X-ray scattering and angle-resolved photoelectron spectroscopies," J. Synchrotron Radiat. **17**, 631–643 (2010).
[26]J. Braun, J. Minár, S. Mankovsky, V. N. Strocov, N. B. Brookes, L. Plucinski, C. M. Schneider, C. S. Fadley, and H. Ebert, Phys. Rev. B **88**, 205409 (2013).
[27]F. F. Y. Wang and K. P. Gupta, "Phase transformation in the oxides," Metall. Trans. **4**, 2767 (1973).
[28]A. Chikina, F. Lechermann, M.-A. Husanu, M. Caputo, C. Cancellieri, X. Wang, T. Schmitt, M. Radovic, and V. N. Strocov, "Orbital ordering of the mobile and localized electrons at oxygen-deficient $LaAlO_3/SrTiO_3$ interfaces," ACS Nano **12**, 7927–7935 (2018).
[29]V. N. Strocov, A. Chikina, M. Caputo, M.-A. Husanu, F. Bisti, D. Bracher, T. Schmitt, F. Miletto Granozio, C. A. F. Vaz, and F. Lechermann, "Electronic phase separation at $LaAlO_3/SrTiO_3$ interfaces tunable by oxygen deficiency," Phys. Rev. Materials **3**, 106001 (2019).
[30]F. Lechermann, H. O. Jeschke, A. J. Kim, S. Backes, and R. Valentí, "Electron dichotomy on the $SrTiO_3$ defect surface augmented by many-body effects," Phys. Rev. B **93**, 121103 (2016).
[31]M. Wu, H. L. Xin, J. O. Wang, X. J. Li, X. B. Yuan, H. Zeng, J.-C. Zheng, and H.-Q. Wang, "Investigation of the multiplet features of $SrTiO_3$in X-ray absorption spectra based on configuration interaction calculations," J. Synchrotron Radiat. **25**, 777–784 (2018).
[32]Q. Zhao and X.-L. Cheng, "Study on the Ti K, $L_{2,3}$ and M edges of $SrTiO_3$ and $PbTiO_3$," J. Phys. Chem. A **124**, 322–327 (2019).
[33]V. N. Strocov, F. Lechermann, A. Chikina, F. Alarab, L. L. Lev, V. A. Rogalev, T. Schmitt, and M.-A. Husanu, "Dimensionality of mobile electrons at x-ray-irradiated $LaAlO_3/SrTiO_3$ interfaces," Electron. Struct. **4**, 015003 (2022).
[34]T. H. Straub, R. Claessen, P. Steiner, S. Hufner, V. Eyert *et al.*, "Many-body definition of a Fermi surface: Application to angle-resolved photoemission," Phys. Rev. B **55**, 13473–13478 (1997).
[35]M. H. Li, H. Li, Y. L. Gan, H. Xu, C. M. Xiong, F. X. Hu, J. R. Sun, T. Schmitt, V. N. Strocov, Y. Z. Chen, and B. G. Shen, "Decoupling the conduction from redox reaction and electronic reconstruction at polar oxide interfaces," Phys. Rev. Mater. **6**, 035004 (2022).
[36]G. van der Laan, J. Zaanen, G. A. Sawatzky, R. Karnatak, and J.-M. Esteva, "Comparison of x-ray absorption with x-ray photoemission of nickel dihalides and NiO," Phys. Rev. B **33**, 4253–4263 (1986).
[37]Z. Wang, S. McKeown Walker, A. Tamai, Y. Wang, Z. Ristic, F. Y. Bruno, A. de la Torre, S. Riccò, N. C. Plumb, M. Shi, P. Hlawenka, J. Sánchez-Barriga, A. Varykhalov, T. K. Kim, M. Hoesch, P. D. C. King, W. Meevasana, U. Diebold, J. Mesot, B. Moritz, T. P. Devereaux, M. Radovic, and F. Baumberger, "Tailoring the nature and strength of electron–phonon interactions in the $SrTiO_3$(001) 2D electron liquid," Nat. Mater. **15**, 835–839 (2016).